Development and characterisation of novel electrospun polylactic acid /tubular clay nanocomposites

Y. Dong [a,*] , D. Chaudhary [b], H. Haroosh [b] and T. Bickford [a]

[a] *Department of Mechanical Engineering, Curtin University of Technology, Perth, WA 6845, Australia*

[b] *Department of Mechanical Engineering, Curtin University of Technology, Perth, WA 6845, Australia*

* Corresponding author. Tel.: +61 8 92669055; fax: +61 8 92662681.

E-mail address: Y.Dong@curtin.edu.au (Y. Dong).

Abstract

A novel material formulation method of polylactic acid (PLA)/tubular clay nanocomposites via electrospinning was introduced and the important processing parameters such as solution concentration, clay loading, material feed rate were particularly investigated. The hybrid fibre diameter, the clay dispersability and the thermal properties of such nanocomposites were then characterised by using the scanning electron microscopy (SEM), wide-angle X-ray diffraction (WAXD) and differential scanning calorimetry (DSC), respectively, to establish a fundamental structure-property relationship for the future application.

Keywords: Electrospinning; PLA/tubular clay nanocomposites; SEM; WAXD; DSC.

1. Introduction

Electrospinning of polymer solutions is a quite versatile process to fabricate

ultrafine micro/nanofibrous structures in the form of non-woven mats. They could be potentially used in the effective drug delivery, tissue scaffolding, nanofiltration system, cosmetics and so on [1, 2]. When the solution jet is released, the polymer droplets are elongated into fibrous structures by an electrostatic force due to the positive charge, which are subsequently attached to the earth ground collector. During the electrospinning process, a cone-like structure is generated at the tip of the capillary, widely known as Talyor cone [3].

Apart from utilisation of base polymers such as polylactic acid (PLA), polycaprolactone (PCL), polyvinyl alcohol (PVA), polymethyl methacrylate (PMMA), etc in electrospinning, recent studies focus on their counterpart composites like PVA/silica composites, PCL/metal composites, nylon 6/clay composites to benefit from the enhancement of multifunctional properties, especially the reinforcement effect [1, 2]. Named after a Belgian geologist Omalius d´Halloy (1783-1875), Halloysite tubular clay ($Al_2Si_2O_5(OH)_4 \cdot nH_2O$) is a unique type of inorganic fillers similar to kaolin, which shows a longitudinal hollow structure by rolling the layers of tetrahedral sheets of silica and octahedral sheets of alumina, and resembles carbon nantubes (CNTs) in geometry with relatively low cost [4, 5]. A wide range of research work has been investigated in mechanical and microstructural properties [6-8], fracture behaviour [8], fire retardancy [9] and thermal properties [7, 10] of polymer/ tubular clay nanocomposites. However, the combined process of electrospinning tubular clay filled nanocomposites is still at the infant stage with very limited work [11] especially when targeting the drug delivery application. The purpose of present work is to report a new fabrication method of PLA/tubular clay nanocomposites in hybrid fibrous formation using electrospinning technique to understand the influence of processing and material parameters, and their

corresponding microstructural and thermal properties.

2. Experimental work

2.1. Materials and fabrication process

Natureworks® PLA (Grade 3051D) pellets for injection moulding application were purchased from Jamplast Inc. (Ellisville, MO USA). The ultrafine premium Halloysite tubular clay particles were donated by Imerys Tableware Asia Limited, New Zealand. Dichloromethane (DCM) was employed to dissolve the PLA along with the additional solvent dimethyl formamide (DMF) to enhance the solution electric conductivity.

PLA pellets were mixed with DCM and DMF in a fixed ratio of 3:1 at room temperature by a bench top orbital shaking incubator for about 3 hrs in order to achieve the PLA solution concentrations of 8 and 12 wt%/v. As-received tubular clays were ultrasonicated for 20 min in DCM solvent which was subsequently evaporated by a hot plate magnetic mixer. The processed tubular clays were vigorously mixed and stirred with PLA solution at room temperature until all the solvents were fully removed. Different clay contents ranging from 0.5, 1, 3 to 5 wt% were used in this study.

The electrospinning process was conducted by transferring the prepared solution into a 10 ml plastic syringe with the luer lock tip to which a 21 gauge hypodermic metal needle was attached. A Fusion 100 syringe pump (Chemyx Inc. Stafford, TX USA) was operated to automatically control the fluid flow at constant feed rates of 1, 2 and 3 ml/hr. The positive electrode of a ES30P–5W high voltage power supply (Gamma High Voltage Research, Ormond Beach, FL USA) running at 25 kV was fixed with the needle via a crocodile clip; whereas a mesh collector covered by aluminium foil was connected to the earth ground point. The distance between the needle tip and the collector was kept at 14 cm. The entire setup was placed in a

transparent acrylic housing case surrounded by a fume cupboard to remove the solvents during electrospinning.

2.2 Microstructural and thermal characterisation

To examine intercalation level of tubular clays, wide angle X-ray diffraction (WAXD) analysis was carried out via Bruker D8 ADVANCE diffractometer (Germany) at 40 kV and 40 mA with Cu-k_α X-ray beam (wave length λ = 0.1541 nm). Mat samples were scanned at 2θ from 5 to 40° in a step size of 0.02°/s.

The surface morphology of electrospun fibre mats was examined by using a Philips XL30 field emission scanning electron microscope at an accelerating voltage of 5 kV. The mat samples were sputter coated with platinum. The SEM micrographs were further evaluated using an imaging analysis tool, ImageJ, developed by National Institutes of Health (NIH), USA to determine the average diameters of electrospun fibres. Approximately 25 fibres per micrograph were chosen and various locations on each fibre were examined to consider possible dimensional non-uniformity of fibres.

Thermal properties of all electrospun mats were determined via differential scanning calorimetry (PerkinElmer DSC 6000, Waltham, Massachusetts USA) from 30 to 200°C at the heating/cooling rate of 10°C/min. The temperature of DSC samples was maintained at 200°C in an isothermal condition for 5 min to eliminate any thermal history. The heating, cooling and reheating cycles were programmed, and the glass transition temperature (T_g), cold crystallisation temperature (T_{cc}), melting temperature (T_m) and heat of fusion (ΔH_m) were measured from the second heating cycle. The degree of crystallinity (X_c) was calculated from [12]

$$X_c(\%) = \frac{\Delta H_m}{\Delta H_m^0} \times \frac{100}{w} \qquad (1)$$

Where $\Delta H_m{}^0$ is the heat of fusion for a 100% crystalline PLA material ($\Delta H_m{}^0$ =93 J/g

[13]) and *w* is the weight fraction of PLA in the prepared mat sample.

3. **Results and discussion**

3.1 XRD analysis

In order to examine the clay content effect, the XRD patterns of as–received tubular clays, electrospun PLA (12%/v) as well as corresponding PLA/clay nanocomposites at the feed rate of 2 ml/hr with various clay contents from 0.5, 1, 3 to 5 wt% are demonstrated in Fig. 1. For tubular clays alone, three characteristic XRD peaks were detected at 2θ =12.10, 19.96 and 24.88°, which are corresponding to the reflection planes of (001), (020), (110) and (002) with *d*-spacing values of 0.731, 0.445 and 0.358 nm, respectively. Due to the existence of first peak (d_{001}= 0.731 nm) and absence of 10Å peak (2θ =8.76°) for hydrated particles, this type of tubular clay is also referred to as (7Å)–Halloysite with almost fully dehydrated formation [6, 8, 14].

At a given PLA solution concentration of 12%/v and relatively low clay contents of below 3 wt%, no apparent sharp peaks occur for PLA/clay nanocomposites with very similar XRD patterns to that of pure PLA. The only distinction could be made based on a non–shifted XRD peak taking place with relative low intensity at 0.5 wt% filled PLA/clay nanocomposites as compared to that of clay at the same 2θ =26.63°. This phenomenon might be attributed to either insufficient diffraction effect or a lack of the formation of well–ordered clay structures at such low clay contents. Quite differently, the first and second reflection (001) peaks of 5 wt% PLA/clay nanocomposites are both shifted to higher angles at 2θ =12.41 and 16.81° with the decreased *d*-spacing values of 0.713 and 0.527 nm, respectively, which might suggest the formation of clay collapsed structure (or “de–intercalation”). Furthermore, the intensity of their second reflection (001) peak has been greatly enhanced, possibly resulting in well–ordered large clay agglomerates as well. Conversely, the reflection

(020), (110) peaks of such nanocomposites are located at lower angle of 2θ =19.20° corresponding to relatively large *d*-spacing value of 0.462 nm in comparison to 0.445 nm for tubular clay. This result reflects the presence of a limited intercalated structure in the clay dispersion. A totally different sign is revealed for the reflection (002) peak where its *d*–spacing value of nanocomposites is almost comparable to that of tubular clay, signifying the non–intercalation effect due to the minimal peak shift.

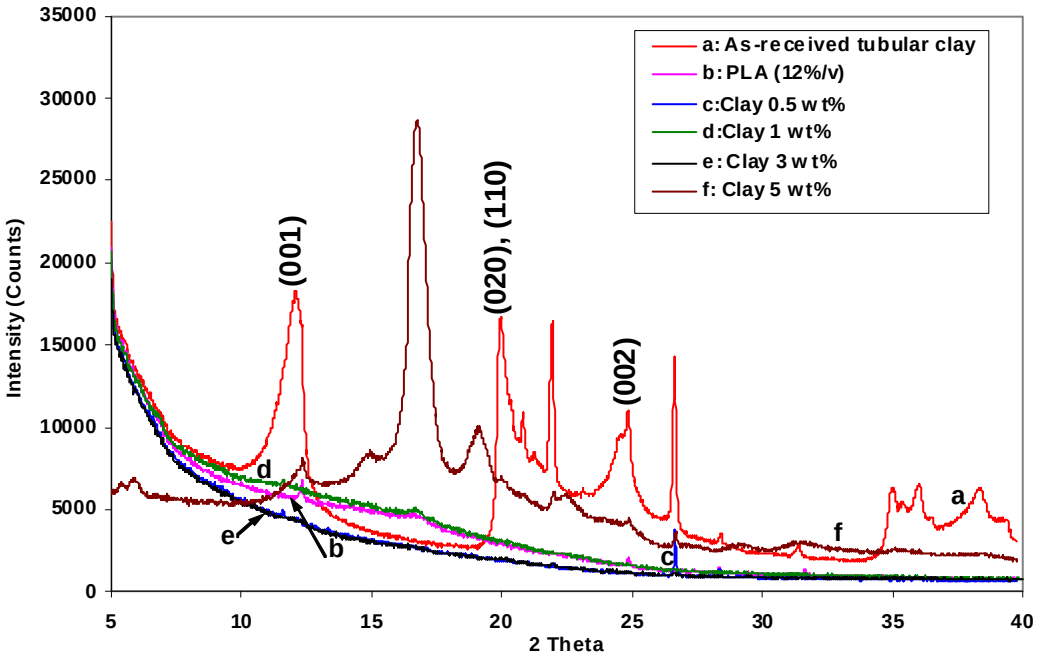

Fig. 1. XRD patterns of (a) as–received tubular clay, (b) electrospun PLA (12%/v) and corresponding electrospun PLA/clay nanocomposites at clay contents of (c) 0.5 wt%, (d) 1 wt%, (e) 3 wt% and (f) 5 wt%.

3.2 SEM characterisation

Fig. 2 demonstrates the different morphological structures of electrospun PLA/clay nanocomposites with the same material formulation used in aforementioned XRD analysis for the further investigation of clay content impact. At the additional clay contents of below 3 wt%, the majority of PLA/clay nanocomposites yield relatively small fibre diameter between 0.3 and 1μm, which could be attributed to both enhancements of electrical conductivity and viscosity of prepared solution due to the inclusion of tubular clay as proven elsewhere [15]. However, a certain degree of

ribbon-like beads with internal pores take place for nanocomposites containing 1 wt% clays. These noticeable defects are most likely due to the flow instability with the formation of droplet rather than fibrous structure [11]. On the other hand, the significant fibre dimensional variation of electrospun nanocomposites has been clearly observed between 3 and 5 wt% clay inclusions. The fibre diameter of 3 wt% clay filled nanocomposites is ranging from 0.8 to 3 μm but the clay dispersion is still very uniform as opposed to 5 wt% nanocomposites; whereas large clay agglomerates and "slurry-like" unfavourable structure co-exist in the morphology of 5 wt% filled nanocomposites, along with non-woven entangled fibres with great diameter variations from 0.5 to 5 μm. Such visual clay aggregation here coincides with the finding of enhanced second reflection (001) peak intensity at the clay content of 5 wt%, Fig. 1. The "slurry-like" structure may be caused by excessive undispersed clay particles to prevent the solution jet from being elongated into fibrous formation.

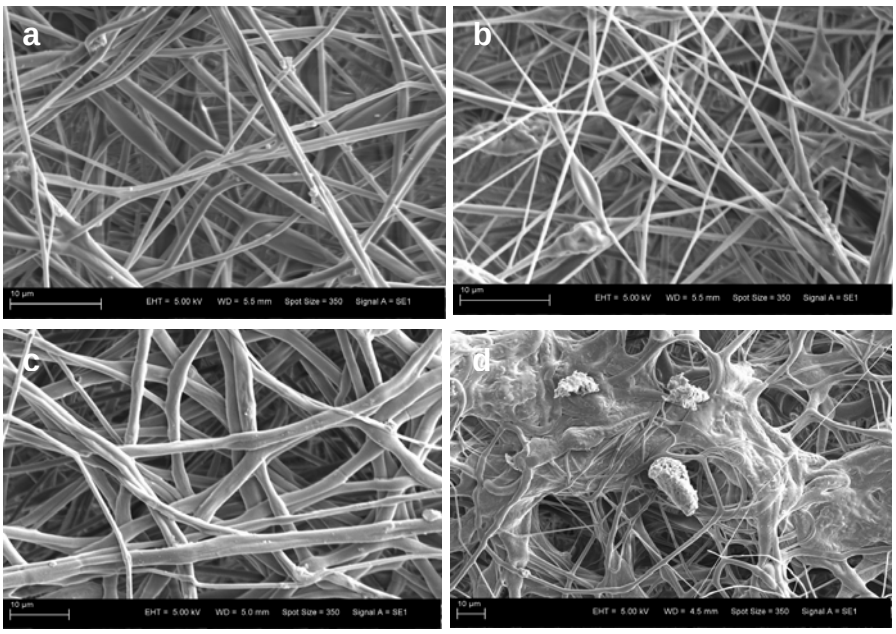

Fig. 2. SEM micrographs of PLA/tubular clay nanocomposites at varied clay contents (PLA: 12%/v and feed rate: 2 ml/hr): (a) 0.5 wt%, (b) 1 wt%, (c) 3 wt% and (d) 5 wt%.

Two major varied processing parameters were also studied in SEM analysis which

comprise the solution concentration of PLA (8%/v and 12%/v) and the feed rate (1, 2 and 3 ml/hr). A series of representative SEM micrographs were illustrated in Fig. 3 under various processing conditions for 0.5 wt% clay filled nanocomposites. The tubular clay particles in range of 200–800 nm for the lateral dimension were embedded into the electrospun fibres with good interfacial interactions. No clear de–bonding or pull-out of particles was found. However, some local clay agglomerates (less than 5 μm) are still visible as shown in Figs. 3(b)–(d). At a given 8%/v for the PLA concentration, the bead formation was predominantly detected with the maximum lateral dimension of over 10 μm at the feed rate of 1 ml/hr. These large beads also concur with entangled fibrous structures down to the fibre diameter of less than 800 nm. More interestingly, the beads have greatly diminished despite relatively non–uniform fibrous structures at 3 ml/hr. When PLA concentration increases up to 12%/v, bead–free fibrous structures become quite manifested regardless of applied different feed rates, which might imply that the viscosity of polymer solution could have greater impact on the electrospun fibre quality as opposed to the feed rate. Taking that fact into consideration, Figs 3(e) and (f) exhibit typical frequency distribution curves of average fibre diameter in nanocomposites only containing PLA solution concentration of 12%/v at feed rates of 1 and 3 ml/hr. To quantify the number of nanofibres with average fibre diameter below 1 μm, it occurs more frequently (shown in Fig. 3(f)) in PLA/clay nanocomposites at feed rate of 3 ml/hr for which the frequency contribution of 88% has been achieved. In particular, more uniform nanofibres in range of 400 to 600 nm and 600 to 800 nm are prevalently detected at 3 ml/hr with the frequency contribution of 76%. On the contrary, electrospun PLA/clay nanocomposites at 1 ml/hr produced much lower number of nanofibres (frequency contribution of 32 %), Fig. 3(e). A most widespread dimensional variation from 0.4 to

2.4 μm was found instead. It is implied that quite a low feed rate might potentially impede the flow stability of solution due to the existence of tubular clays and optimal feed rate of 3 ml/hr appears to be more feasible in such electrospinning process.

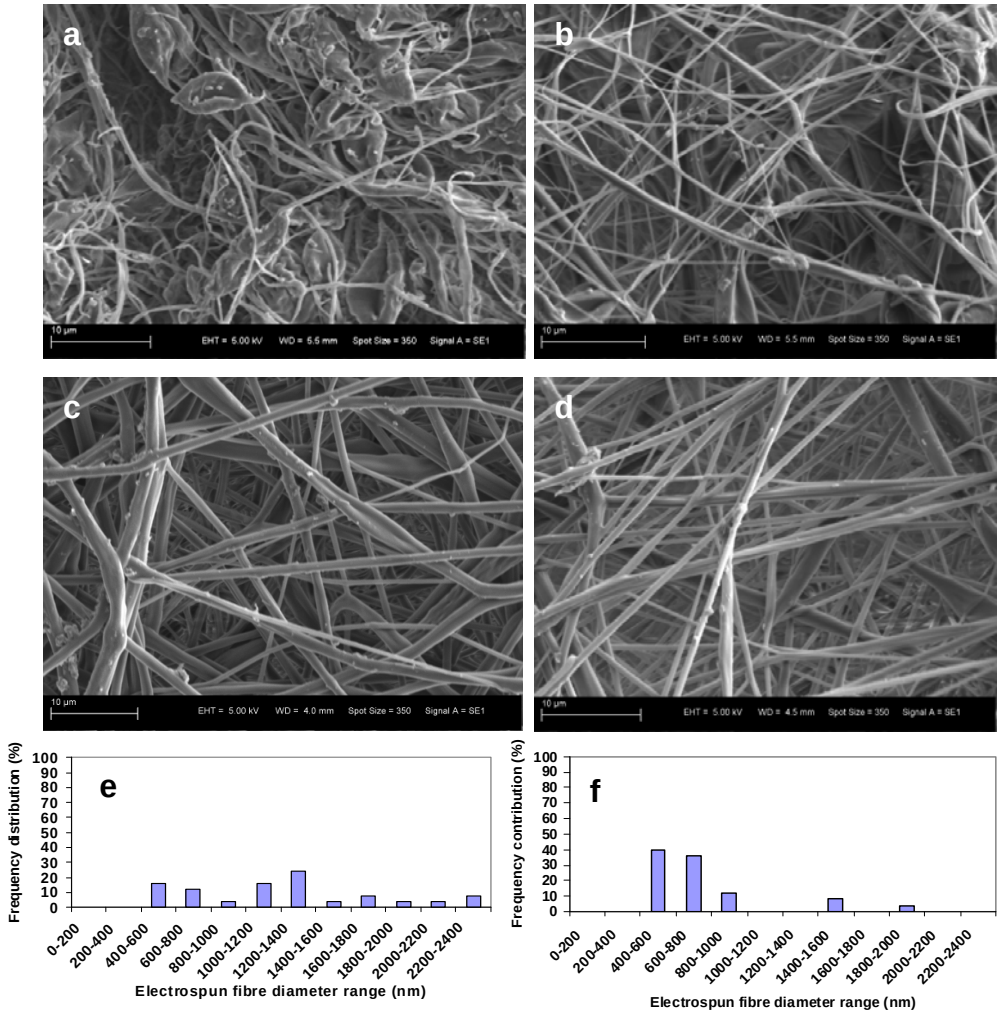

Fig. 3. SEM micrographs of 0.5% filled PLA/tubular clay nanocomposites at varied processing parameters: (a) PLA (8%/v) and feed rate of 1 ml/hr, (b) PLA (8%/v) and feed rate of 3 ml/hr,(c) PLA (12%/v) and feed rate of 1 ml/hr, (d) PLA (12%/v) and feed rate of 3 ml/hr and typical frequency distributions of electrospun 0.5 wt% filled PLA/clay nanocomposites (PLA: 12%/v) at varied feed rates: (e) 1 ml/hr and (f) 3 ml/hr.

3.3 DSC measurement

All DSC thermograms of electrospun PLA (12%/v) and PLA/ clay nanocomposites at the clay contents from 0.5 to 5 wt% are plotted in Fig. 4 along with the summarised

characteristic parameters in Table 1 accordingly. Similar glass transition temperatures were found for all DSC samples of PLA /clay nanocomposites regardless of the clay content, which are also comparable to that of PLA (T_g = 59.28°C). Cold crystallisation temperatures decrease remarkably to 114-117°C at the low clay contents (0.5 to 3 wt%) when compared with T_{cc} of PLA at 123.80°C. This behaviour can be explained by the effective nucleating agent role of well dispersed clays as depicted in Figs. 2(a) and (c), thus causing their strong interaction with the PLA matrix to enhance its nucleation level and crystal growth rate [16-18]. PLA molecules with a small amount of well dispersed additional clays are believed to facilitate the crystallisation process occurring at lower temperatures, resulting in the subsequent decrease of T_{cc}. Interesting to see, T_{cc} of such nanocomposites has drastically changed at the clay content of 5 wt% and even becomes slightly higher than that of PLA. The relatively high clay content might lead to constraints and partial immobilisation of a large number of PLA molecular chains by attaching to more individual clay particles [18]. The large clay agglomerates found in Fig. 2(d) as physical hindrance would also be detrimental to the PLA crystallisation process due to the non-homogeneous dispersion. The great improvements of degree of crystallinity (X_c) in 0.5–3 wt% filled PLA/clay nanocomposites were shown with nearly five fold values relative to 8.5% for PLA alone. These results agree quite well with corresponding cold crystallisation temperatures, further proving the positive nucleation effect from tubular clays at low content levels. When the clay content increases up to 5 wt%, the degree of crystallinity (X_c =2.8%) is abruptly lowered. The melting temperatures (T_m) follow quite similar tendencies to the degree of crystallinity, being much higher for 0.5-3 wt% clay inclusions but remaining comparable to PLA at 5 wt%. This finding might shed light on the potential use of tubular clays to improve the thermal stability and

inflammability level of PLA significantly as evidenced elsewhere [19, 20].

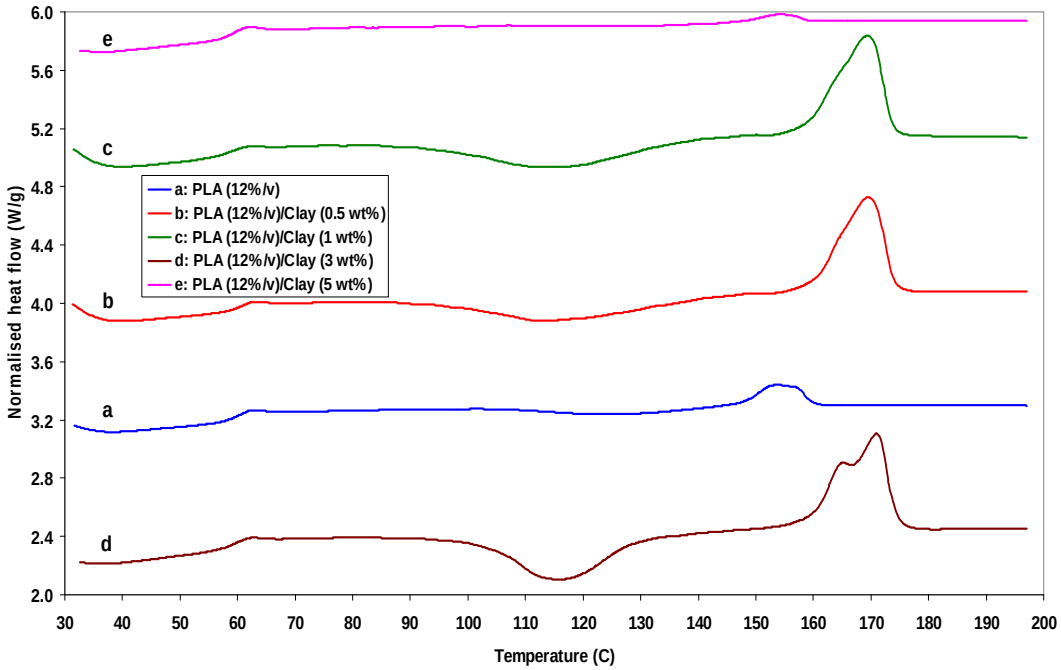

Fig. 4. DSC thermograms of PLA and PLA/clay nanocomposites: (a) PLA (12%/v), (b) PLA (12%/v)/ clay (0.5 wt%), (c) PLA (12%/v)/ clay (1 wt%), (d) PLA (12%/v)/ clay (3 wt%) and (e) PLA (12%/v)/ clay (5 wt%).

Table 1 DSC characteristic parameters for PLA and PLA/clay nanocomposites

DSC samples	Clay content (wt %)	T_g (°C)	T_{cc} (°C)	T_m (°C)	ΔH_m (J/g)	X_c (%)
PLA (12%/v)	0	59.28	123.80	153.77	7.91	8.5
PLA (12%/v)/ clay (0.5 wt%)	0.5	60.20	114.49	169.38	35.18	38.0
PLA (12%/v)/ clay (1 wt%)	1	59.35	116.80	169.54	38.28	41.6
PLA (12%/v)/ clay (3 wt%)	3	60.10	115.79	170.98	38.72	42.9
PLA (12%/v)/ clay (5 wt%)	5	59.54	127.28	154.11	2.46	2.8

Conclusions

A novel material formulation in electrospinning process was developed by incorporating tubular clays at low content levels from 0.5 to 5 wt% with PLA. Such PLA/tubular clay nanocomposites show good clay dispersion for 0.5 to 3 wt% clay inclusions as evidenced by weak XRD peaks and SEM morphological structures. At

the clay content of 5 wt%, a complex dispersion status is yielded with de-intercalated, limited intercalated and non–intercalated effects taking place at reflection (001), (020), (110) and (002) peaks, respectively. In addition, large clay agglomerates and "slurry-like" unfavourable structure are confirmed in SEM analysis for 5 wt% filled nanocomposites as well. The study of varied processing parameters suggests that higher solution concentration of PLA (12%/v) and fast feed rate (3 ml/hr) contribute greatly to the dimensional uniformity and bead-free formation of fibrous structures. The enhancement of thermal properties such as melting temperature (T_m) and degree of crystallinity (X_c) is quite attractive for 0.5-3 wt% filled nanocomposites. The lower cold crystallization temperature (T_{cc}) at similar clay content levels is ascribed to the effective nucleating agent role of tubular clays. However, for nanocomposites containing 5 wt% clays, X_c and T_{cc} are drastically altered to reach a similar level to those for electrospun PLA, possibly arising from the non-uniform clay dispersion with relatively high clay content and large agglomerates. This work could offer a clear insight to shift the real applications of tubular clays from conventional reinforcements to drug delivery in the future when both their hollow structure as potential carrier and electrospinning nanofibre technique are considered.

Acknowledgements

The authors would like to thank the financial supports from both Curtin Internal Research Grants (IRG) 2010 (Project No.: 47604) and New Staff Academic Development Fund to Dr. Y. Dong. The technical assistance of XRD analysis from Prof. De Yu Li, Centre for Materials Research (CMR), Curtin University of Technology is also acknowledged.

References

[1] Huang ZM, Zhang YZ, Kotaki M, Ramakrishna S (2003) Compos Sci Technol 63 : 2223-2253.
[2] Agarwal S, Wendorff JH, Greiner A (2008) Polymer 49:5603-5621.
[3] Inai R, Kotaki M, Ramakrishna S (2005) Nanotechnology 16: 208-213.
[4] Joussein E, Petit S, Churchman J, Theng B, Righi D, Delvaux B (2005) Clay Miner 40: 383-426.
[5] Harvey CC, Murray HH (1990) Clay Miner Soc Spec Pub 1: 233-248.
[6] Ismail H, Pasbakhsh P, Ahmad Fauzi MN, Abu Bakar A (2009) Polym-Plast Technol Eng 48: 313-323.
[7] Ismail H, Pasbakhsh P, Ahmad Fauzi MN, Abu Bakar A (2008) Polym Test 27: 841-850.
[8] Deng S, Zhang J, Ye L. Compos Sci Technol (2009) 69: 2497-2505.
[9] Marney DCO, Russell LJ, Wu DY, Nguyen T, Crammb D, Rigopoulos N, Wright N, Greaves M (2008) Polym Degrad Stabil 93: 1971-1978.
[10] Liu M, Guo B, Zou Q, Du M, Jia D (2008) Nanotechnology 19: 205709.
[11] Touny AH, Lawrence JG, Jones AD, Bhaduri SB (2010) J Mater Res 25: 857-865.
[12] Matthew AP, Oksman K, Sain M (2006) J Appl Polym Sci 101: 300-310.
[13] Fischer EW, Sterzel HJ, Wegner G, Kolloid ZZ (1973) Polymer 251: 980-990.
[14] Levis SR, Deasy PB (2002) Int J Pharm 243: 125-134.
[15] Marras SI, Kladi KP, Tsivintzelis I, Zuburtikudis I, Panayiotou C (2008) Acta Biomater 4: 756-765.
[16] Lee JH, Park TG, Park SH, Lee DS, Lee YK, Yoon SC, Nam JD (2003) Biomaterial 24: 2773-2778.
[17] Chow WS, Lok SK (2009) J Therm Anal Calorim 95: 627-632.
[18] Di Y, Iannace S, Maio ED, Nicolais L (2005) J Polym Sci Pt B-Polym Phys 43 : 689-698.
[19] Ning N, Yin Q, Luo F, Zhang Q, Du R, Fu Q (2007) Polymer 48 : 7374-7384.
[20] Du M, Guo B, Jia D (2006) Eur Polym J 42: 1362-1369.

List of Figures

Fig. 1. XRD patterns of (a) as–received tubular clay, (b) electrospun PLA (12%/v) and corresponding electrospun PLA/clay nanocomposites at clay contents of (c) 0.5 wt%, (d) 1 wt%, (e) 3 wt% and (f) 5 wt%.

Fig. 2. SEM micrographs of PLA/tubular clay nanocomposites at varied clay contents (PLA: 12%/v and feed rate: 2 ml/hr): (a) 0.5 wt%, (b) 1 wt%, (c) 3 wt% and (d) 5 wt%.

Fig. 3. SEM micrographs of 0.5% filled PLA/tubular clay nanocomposites at varied processing parameters: (a) PLA (8%/v) and feed rate of 1 ml/hr, (b) PLA (8%/v) and feed rate of 3 ml/hr,(c) PLA (12%/v) and feed rate of 1 ml/hr, (d) PLA (12%/v) and feed rate of 3 ml/hr and typical frequency distributions of electrospun 0.5 wt% filled PLA/clay nanocomposites (PLA: 12%/v) at varied feed rates: (e) 1 ml/hr and (f) 3 ml/hr.

Fig. 4. DSC thermograms of PLA and PLA/clay nanocomposites: (a) PLA (12%/v), (b) PLA (12%/v)/ clay (0.5 wt%), (c) PLA (12%/v)/ clay (1 wt%), (d) PLA (12%/v)/ clay (3 wt%) and (e) PLA (12%/v)/ clay (5 wt%).

List of Tables

Table 1 DSC characteristic parameters for PLA and PLA/clay nanocomposites